



Swansea University
Prifysgol Abertawe



Cronfa - Swansea University Open Access Repository

This is an author produced version of a paper published in :
The British Journal of Radiology

Cronfa URL for this paper:
<http://cronfa.swan.ac.uk/Record/cronfa30155>

Paper:

Almatani, T., Hugtenburg, R., Lewis, R., Barley, S. & Edwards, M. (2016). Automated algorithm for CBCT-based dose calculations of prostate radiotherapy with bilateral hip prostheses. *The British Journal of Radiology*, 89(1066), 20160443
<http://dx.doi.org/10.1259/bjr.20160443>

This article is brought to you by Swansea University. Any person downloading material is agreeing to abide by the terms of the repository licence. Authors are personally responsible for adhering to publisher restrictions or conditions. When uploading content they are required to comply with their publisher agreement and the SHERPA RoMEO database to judge whether or not it is copyright safe to add this version of the paper to this repository.

<http://www.swansea.ac.uk/iss/researchsupport/cronfa-support/>

1 Automated algorithm for CBCT-based dose
2 calculations of prostate radiotherapy with
3 bilateral hip prostheses
4

5 Turki Almatani^{1,*}, Richard P. Hugtenburg^{1,2}, Ryan D. Lewis²,
6 Susan E. Barley³, and Mark A. Edwards²

7 ¹College of Medicine, Swansea University, Singleton Park, Swansea SA2 8PP, UK

8 ²Department of Medical Physics and Clinical Engineering, Singleton Hospital, ABM
9 University Health Board, Swansea SA2 8QA, UK

10 ³Oncology Systems Limited, 14 Longbow Close, Shrewsbury SY1 3GZ, UK

11
12
13
14
15
16
17
18
19
20
21
22
23
24
25
26
27
28
29
30
31
32
33
34
35
36
37

*Corresponding author. E-mail address: turkialmatani@gmail.com (T. Almatani)

38 **Objective:** Cone beam CT (CBCT) images contain more scatter than a conventional CT
39 image and therefore provide inaccurate Hounsfield units (HU). Consequently CBCT
40 images cannot be used directly for radiotherapy dose calculation. The aim of this study is
41 to enable dose calculations to be performed with the use of cone-beam CT images taken
42 during radiotherapy and evaluate the necessity of re-planning.

43 **Methodology:** A prostate cancer patient with bilateral metallic prosthetic hip
44 replacements was imaged using both CT and CBCT. The multilevel threshold algorithm
45 (MLT) was used to categorise pixel values in the CBCT images into segments of
46 homogeneous HU. The variation in HU with position in the CBCT images was taken into
47 consideration. This segmentation method relies upon the operator dividing the CBCT
48 data into a set of volumes where the variation in the relationship between pixel values
49 and HUs is small. An automated MLT algorithm was developed to reduce the operator
50 time associated with the process. An intensity modulated radiation therapy (IMRT) plan
51 was generated from CT images of the patient. The plan was then copied to the segmented
52 CBCT data sets with identical settings and the doses were recalculated and compared.

53 **Results:** Gamma evaluation showed that the percentage of points in rectum with $\gamma < 1$
54 (3%/3 mm) were 98.7% and 97.7% in the segmented CBCT using MLT and the
55 automated MLT algorithms, respectively. Compared with the planning CT (pCT) plan,
56 the MLT algorithm showed -0.46% dose difference with 8 hours operator time while the
57 automated MLT algorithm showed -1.3%, which are both considered to be clinically
58 acceptable, when using collapsed cone (CC) algorithm.

59 **Conclusion:** The segmentation of CBCT images using the method in this study can be

60 used for dose calculation. For a prostate patient with bilateral hip prostheses and the
61 associated issues with CT imaging, the MLT algorithms achieved a sufficient dose
62 calculation accuracy that is clinically acceptable. The automated MLT algorithm reduced
63 the operator time associated with implementing the MLT algorithm to achieve clinically
64 acceptable accuracy. This saved time makes the automated MLT algorithm superior and
65 easier to implement in the clinical setting.

66 **Advance in knowledge:** The MLT algorithm has been extended to the complex example
67 of a patient with bilateral hip prostheses, which with the introduction of automation is
68 feasible for use in ART, as an alternative to obtaining a new planning CT and re-
69 outlining the structures.

70

71

72

73

74

75

76

77

78

79

80

81

82

83 **1 Introduction**

84 One of the desirable objectives during external beam radiotherapy (EBRT) of the prostate
85 is the delivery of an uniform radiation dose to the treatment volume while sparing organs
86 at risk. In practice, this may be difficult to achieve due to day-to-day changes in patient
87 positioning, patient shape and internal organ movement during the treatment course (1).
88 Interfractional motions such as variations in bladder and rectum volume have been
89 demonstrated to have significant effects on prostate position and a negative impact on the
90 accuracy of the treatment course (2).

91 The implementation of image guided radiation therapy (IGRT) in clinical practice, such
92 as kilovoltage cone beam computed tomography (kV-CBCT), has improved tumor
93 targeting and tumour control during the treatment delivery process and reducing dose
94 delivery to normal tissues. CBCT has been used to correct patient set-up in the treatment
95 position and to monitor any anatomical deformations in 3D with sufficient soft tissue
96 contrast (3). In addition, CBCT can be feasible for adaptive radiotherapy (ART), e.g.
97 dose recalculation, if the Hounsfield units (HU) are accurate and reliable (4).

98 Due to its cone-beam geometry, the amount of scatter in CBCT images is greater than
99 that of conventional CT images (fan beam),and is dependent on the scanned object size,
100 the collimator and the filter used (5). The image quality also depends on acquisition
101 parameters, i.e. mA, kV and the number of projections. In addition, limited gantry
102 rotation speed and large field-of-view (FOV) in a single rotation reduce image quality.
103 Therefore, CBCT images provide inaccurate HUs and, consequently, cannot be used
104 directly for dose calculation (6). Therefore, if there are significant anatomical changes

105 observed on the CBCT images, acquiring another CT is necessary for an accurate
106 assessment of dose differences. This procedure is time consuming across all staff groups
107 involved in the radiotherapy pathway and additional dose is delivered to the patients.
108 Thus it would be sufficient to use CBCT images that were already taken during
109 radiotherapy for evaluating the necessity of re-planning. Many papers have studied the
110 use of CBCT data for dose recalculation, which is still an active area for research (6).

111 To deal with HU calibration of CBCT images, Richter et al (2008) proposed a method
112 where HU-electron density conversion curves were based on average CBCT HU values
113 for separate treatment sites in order to generate population-specific conversion curves (7).
114 Such an approach is still subject to CBCT artefacts and can result in dose calculation
115 errors of greater than 5% when compared to planning CT (pCT) -based dose calculation
116 (6). Some studies deal with correcting scatter by applying quite unsophisticated software
117 corrections to CBCT images before reconstruction (8). Such a method may be unable to
118 accurately reconstruct higher-density material for a large scanned object size. In addition,
119 it may be difficult to implement such a method in a clinic even though recent commercial
120 software releases provide sophisticated scatter correction algorithms (9).

121 Other studies deal with adjustment techniques to correct CBCT HU values, such as
122 mapping the HUs in CT images to the equivalent points in the CBCT image geometry
123 after rigid or deformable image registration (10,11). In addition, image cumulative
124 histograms can be used to adjust HU values between pCT and CBCT images (10).
125 Another technique uses a multilevel- threshold (MLT) algorithm as proposed by Boggula
126 et al (2007), where the pixel values of CBCT images were replaced with a small number
127 of fixed HU values as in CT for air, soft- tissue and bone (12-14). Onozato et al (2014)

128 excluded water and used fat and muscle instead, resulting in a dosimetric difference
129 below 2% (14). In addition, Fotina et al (2008) used the same technique, calling it a
130 density override technique, but with a range of HU values for bone (soft bony structures,
131 hard bone and teeth) and air/low density regions (rectal balloon and lung). All other
132 regions are assumed to be water-equivalent assigned with one HU value, resulting in a
133 dosimetric difference below 2% (6).

134 Recently, Dunlop et al (2015) assessed the CBCT dose calculation accuracy for density
135 override approaches for four pelvis cases, where CBCT voxels were assigned as water
136 only and then as either water or bone (water only and water-and-bone methods). This was
137 then compared with a scatter correction and automated density override approach that is
138 available in the RayStation TPS (V3.99, RaySearch Laboratories, Stockholm,
139 Sweden)(9). In the automated density override approach, six different densities (air, lung,
140 adipose tissue, connective tissue, cartilage/bone, and higher density for prosthesis) are
141 assigned to the CBCT image by binning the CBCT image histogram into six density
142 levels. Compared with pCT acquired on the same day as the CBCT, the results showed
143 that the automated approach was superior to the other methods, when considering smaller
144 patients (with anterior-posterior distance < 25 cm). For larger patients, the water only
145 method gave the best accuracy.

146 The occurrence of inhomogeneities in the patient anatomy, e.g. hip replacements, has the
147 ability to complicate the automated process, requiring the addition of additional set
148 densities. In fact, none of the above studies used a patient with prostheses, which would
149 provide a more general assessment of dose calculation using CBCT. Almatani et al
150 (2016) studied CBCT-based dose calculations of a prostate patient with a single hip

151 prosthesis using the MLT algorithm. The work showed that it was necessary to extend the
152 MLT algorithm to categorise pixel values into segments on a region-by-region basis, with
153 the region size changing depending on the anatomical features (15). In addition, a larger
154 number of materials (up to 8) than typically used in previous works was explored. The
155 results showed that five values of HU (air, adipose, water, cartilage/bone and metal
156 implant) gave the best balance between dose accuracy (-1.9%) and operator time (5
157 hours). However, the length of operator time needed could make it difficult to implement
158 this as a technique in the clinic.

159 The aim of this work is to develop a more robust method to account for the full range of
160 patient size as well as the difficulties presented by the metal artefacts in both pCT and
161 CBCT images. A CBCT-based dose calculation of a patient with bilateral metal hip
162 prostheses is presented using the extended MLT algorithm, in the same manner extending
163 upon proposed previously by the authors for a single hip prosthesis. In addition, an
164 automated MLT algorithm was developed to reduce the operator time associated with the
165 manual MLT algorithm. With the flexibility of a region-by-region approach, it is
166 envisaged that the method can be applicable for the automation of dose calculation on
167 segmented magnetic resonance (MR) images and could be of interest to MR-based ART
168 (9).

169 **2 Method and materials**

170 **2.1 CBCT image acquisition**

171 The X-ray volumetric imaging integrated in an Elekta Synergy linear accelerator (XVITM,
172 version 4.5, Elekta, Crawley, West Sussex, UK) was used to acquire CBCT images. The

173 CBCT scans were acquired with a field of view (medium FOV) of 41 cm in diameter and
174 17.85 cm in the axial direction with a bowtie filter added (F1). CBCT images were
175 reconstructed with 1 mm cubic voxels and averaged in the longitudinal direction for 3
176 mm slice thickness. The images were then transferred to the Oncentra MasterPlan (OMP)
177 treatment planning system (version 4.3 Elekta, Netherlands) via DICOM protocol for
178 dose calculation.

179 **2.2 Patient study**

180 This study was performed on a patient with bilateral metal hip prostheses replacement
181 treated at the Department of Clinical Oncology and Radiotherapy, South West Wales
182 Cancer Centre ABM University Health Board, Swansea, Wales. The anterior-posterior
183 (AP) separation of the patient was 26.5 cm. Such a challenging case provides a good
184 assessment of dose calculation using CBCT due to the difficulties presented by the metals
185 artefacts in both pCT and CBCT images. The artefacts in pCT were reassigned as water
186 in the original patient plan using a bulk density correction (Fig. 1a). An intensity
187 modulated radiotherapy (IMRT) treatment with five 6-MV photon fields, at gantry angles
188 of 35°, 145°, 180°, 235°, and 300° was performed. The prescription dose was 70 Gy in 35
189 fractions. Dose distribution was calculated using pencil beam (PB) and collapsed cone
190 (CC) algorithms to allow the comparison with Monte Carlo (MC) algorithm and to
191 identify the effects of HU on dose calculation.

192 **2.3 Modification of CBCT images**

193 The MLT algorithm, used to correct CBCT data, involves categorising pixel values in the

194 CBCT images into segments of homogeneous HU using MATLAB scripts (Mathworks,
195 Natick, MA) to generate segmented CBCT (sCBCT) data. Based on Almatani et al
196 (2016), the binning of CBCT images of a patient with hip prosthesis into five HU values
197 results in sufficiently accurate and clinically acceptable dose distribution (15).
198 Considering more than five HU values provides more anatomical information and
199 improves dose calculation accuracy (by 0.23%) but would require more operator time
200 (58%), as the sensitivity increases when increasing the number of HU bins to define the
201 material type. Therefore, in this study, five values of HU values were used to segment
202 CBCT images that represent, air (-976 HU), adipose tissue (- 96 HU), water (0 HU), 2/3
203 cartilage & 1/3 bone (528 HU) and metal implants (2976 HU). The ranges of pixel values
204 in the CBCT images were: air (0 to 200), adipose tissue (201 to 700), water (701 to 875),
205 2/3 cartilage & 1/3 bone (876 to 1600) and metal implant (1601 to 8000).

206 The threshold values for each material at these intervals are dependent on the geometry
207 since noise and scatter in CBCT is variable, especially in the presence of high density
208 materials, as shown in Figure 1(b) (16). In this study, the MLT algorithm was used in two
209 ways, using a manual and an automated procedure. In the manual procedure, the CBCT
210 images were divided into regions with sets of different threshold values, which are
211 determined on a region-by-region basis, to sufficiently correct for the artefacts. The shape
212 of each region is a rectangular cuboid. In general, the greater the variation in the scatter,
213 the greater the number of regions that need to be considered, and the size of the region
214 decreases as it gets closer to inhomogeneities. The resultant segmented CBCT images
215 using this procedure are referred to as sCBCT_{man}.

216 In the automated procedure, the CBCT images were divided into five concentric rings,
217 which are uniform in shape through all slices, using MATLAB scripts, as shown in
218 Figure 1(d). The centre of the inner radius (radius 1) was defined at the centre of the
219 patient geometry, which can be changed by the user. The lower threshold values for each
220 material changes with the radius but is easily determined by the user's analysis of the
221 central slice. For example, the lower threshold value for water, in the inner radius, was
222 defined in relation to the pixel value with the maximum frequency in the slice according
223 to the ratio of the lower threshold value of water and the pixel value with the maximum
224 frequency in the central slice. The same procedure was applied for each material in each
225 radius. The resultant segmented CBCT images using this procedure are referred to as
226 sCBCT_{auto}.

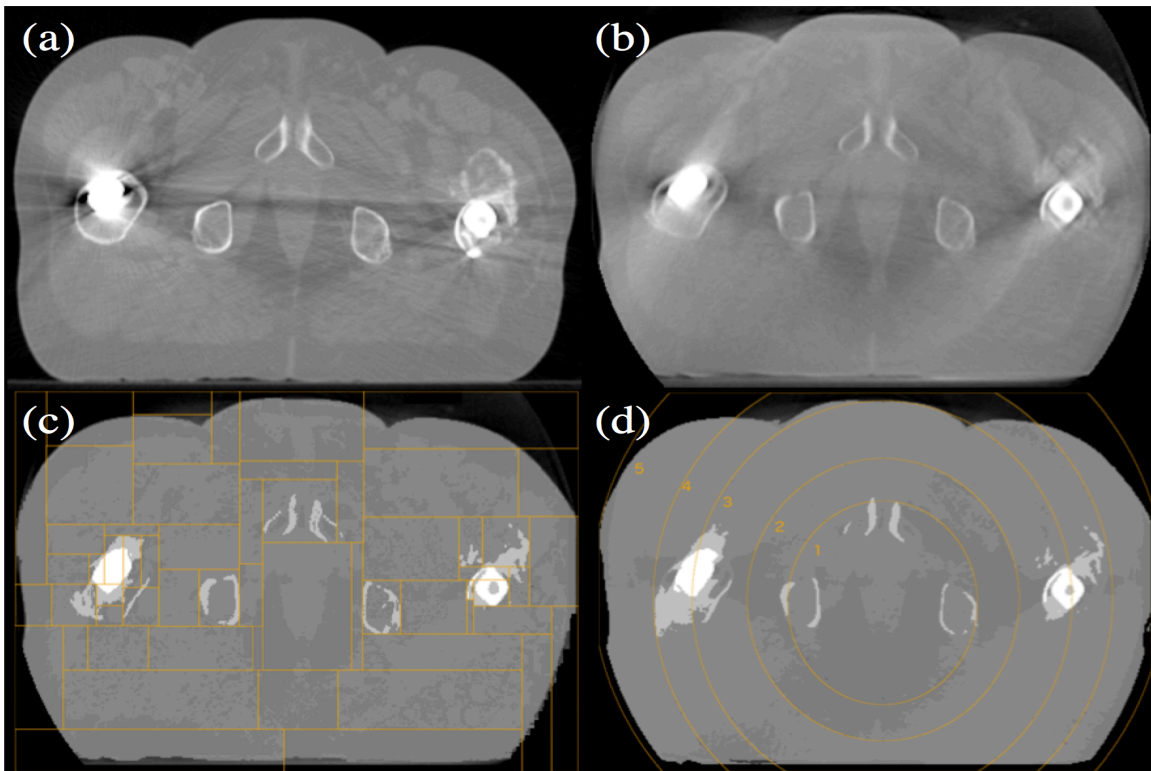


Figure 1: A slice of the pCT (a) and the original CBCT (b) and the resultant images after segmentation CBCT using the manual MLT (sCBCT_{man}) and the automated MLT (sCBCT_{auto}) (c and d respectively).

227 The use of a radial shape was motivated by the fact that, in CBCT, the issue of the
228 scatter occurs spherically and ring artefacts that caused by miscalibrated detector pixel
229 lines/rows, elements or manufacturing defects at a fixed location in the flat panel detector
230 (FPD). In addition, due to the presence of the bilateral hip, the low energetic X-rays are
231 absorbed, thus the polychromatic beam becomes gradually harder. Consequently, the
232 FPD exhibits pixel-to-pixel sensitivity variations, that lead to ring artefacts (17). In a
233 pelvic region with prostheses, there is a rapid change in the exposure to the FPD from
234 frame to frame, receiving high exposure then followed by low exposure due the strong
235 attenuation of the metal. This leads to so-called radar artefacts that appear as a circular
236 radar bright-shaded region, owing to inconsistencies in detector signal and/or gain (18).

237 **2.4 Monte Carlo calculation**

238 The Elekta Synergy linear accelerator was modeled using Electron Gamma Shower
239 (EGSnrc), which is one of the most popular MC codes for medical physics (19).
240 BEAMnrc and DOSXYZnrc are two applications in EGSnrc code that are used to
241 simulate the beam generated from the treatment head and to score dose deposition in
242 voxel grids, respectively. In this study, 90 million particles were used for each beam to
243 provide an accurate simulation with a low statistical uncertainty. High performance
244 computing (HPC-Wales) was used to speed up MC calculations (20). The MC
245 normalization was performed by calculating the dose in a water phantom under the
246 standard reference conditions (10 ×10 field size, 100 cm source-to-surface distance, 5 cm
247 depth).

248 **2.5 Treatment planning evaluation and comparison**

249 The sCBCT (both sCBCT_{man}, sCBCT_{auto}) and pCT images fusion was accomplished with
250 manual rigid registration using ProSoma software (v3.3, MedCom, Germany) and the
251 structure sets were then transferred to the sCBCT images without any modification
252 except the external contour. The plans were then copied to sCBCT using the same
253 geometry and MU values and doses were recalculated using PB and CC algorithms. For
254 MC calculation, the pCT artefacts, caused by the presence of the hip prostheses, were
255 changed to a water material of uniform density using a MATLAB script. The MC dose
256 calculation was then performed on pCT and sCBCT images using the same HU-ED
257 calibration as in OMP. The MC dose file (.3ddose) and the DICOM-RT file were then
258 imported into the computational environment for radiotherapy research (CERR) software
259 to compare the resultant dose distribution (21). Dose volume histograms (DVH) were
260 compared between pCT and sCBCT plans. The maximum dose (D_{max}), mean dose
261 (D_{mean}) and minimum dose (D_{min}) parameters for PTV (prostate and seminal vesicles),
262 rectum and bladder were compared. The coverage of the PTV, the dose to 95% of the
263 PTV ($D_{95\%}$) and the relative volume doses delivered to the rectum and bladder (V_{65} and
264 V_{70}) were compared. In addition, the volume of right/left hip and bone were calculated
265 in the pCT scan and compared with those in the sCBCT_{man} and sCBCT_{auto} scan to show
266 how close the two scans were. To quantitatively appraise the differences between pCT
267 and sCBCT plans, especially for the PTV, rectum and bladder, a gamma index analysis
268 was performed using the pCT plan as a reference. The criteria were set as 3 mm distance
269 to agreement (DTA) and 3% dose difference (DD) and 5% low dose threshold. The
270 conformity index (CI) was calculated for all sCBCT plans and then compared with the
271 pCT plans using PB, CC and MC algorithms (22). In addition, the dose at the isocentre

272 (at the geometric centre of the prostate PTV (PTV_p)) was compared between the pCT and
273 sCBCT_{man} and sCBCT_{auto} plans.

274 3 Results and discussion

275 Figure 2 shows the cross-plane profile/x profile of pCT, sCBCT_{man} and sCBCT_{auto} at the
276 depth of the plan isocentre as well as the CT number of the pCT, sCBCT_{man} and
277 sCBCT_{auto} scans at that depth. In general, the sCBCT_{man} and sCBCT_{auto} profiles are in
278 good agreement with the pCT profile especially at the implant/tissue interface. For bone
279 regions, the sCBCT_{auto} numbers showed less agreement with pCT numbers, compared
280 with sCBCT_{man} numbers where some of these regions were considered as water. In
281 addition, the sCBCT_{auto} overestimated some adipose tissue regions and considered it as
282 water, especially in the PTV region (high-dose region), leading to an underestimation of
283 the dose in that region by -4.4%. On the other hand, sCBCT_{man} numbers considered more

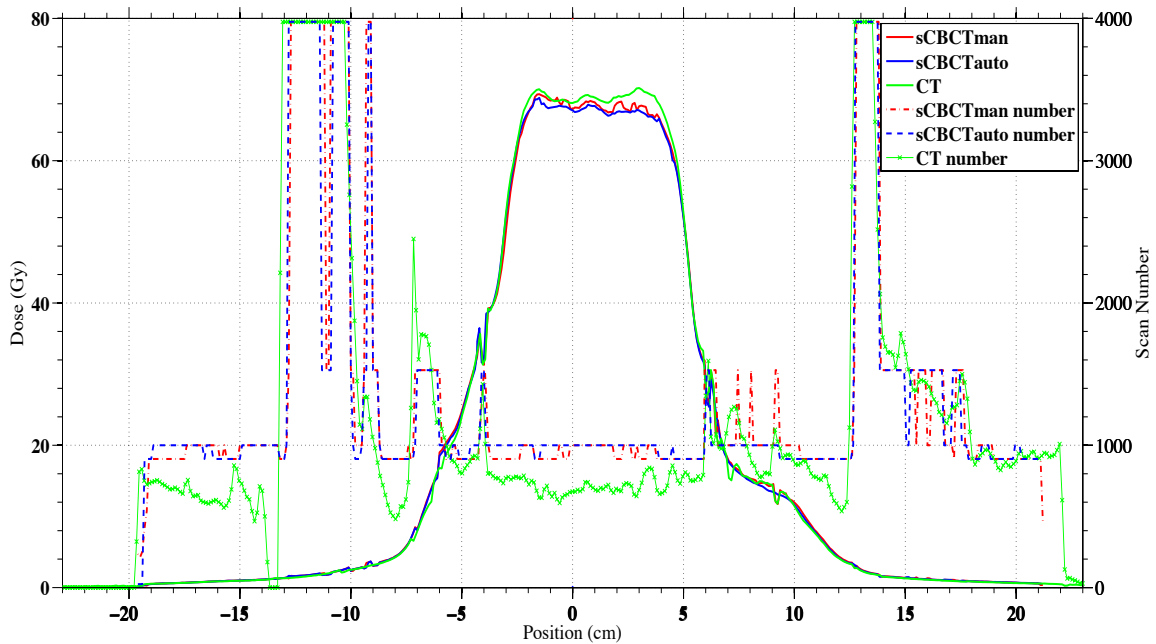


Figure 2: Comparison of the dose profile of pCT, sCBCT_{man} and sCBCT_{auto} plans at the isocentre depth using MC algorithm. The second y axis represents the sCBCT_{man} number, sCBCT_{auto} number and CT number.

284 adipose tissue than $sCBCT_{auto}$ numbers, thus the dose difference with the pCT dose
 285 profile was less when compared with the $sCBCT_{auto}$ dose profile. The largest difference
 286 between the pCT and $sCBCT_{man}$ and $sCBCT_{auto}$ plans was in the PTV region where pCT
 287 was 69.1 Gy, $sCBCT_{man}$ was 66.1 Gy and $sCBCT_{auto}$ was 65.8 Gy when using MC
 288 algorithm.

289 Figure 3 shows the differences in the right (RT)/left (LT) hip and bone volumes
 290 between the pCT scan, $sCBCT_{man}$ and $sCBCT_{auto}$ scans. Compared with the pCT scan,
 291 the largest difference between $sCBCT_{man}$ and $sCBCT_{auto}$ was found in the LT hip where
 292 in $sCBCT_{man}$ it was overestimated by 6.8% and underestimated by -30.2% in $sCBCT_{auto}$.
 293 This underestimation was due to the fact that the automated MLT algorithm was unable
 294 to accurately correct cupping artefacts due to the increased amount of scatter and beam
 295 hardening inside the LT hip, resulting in dark streaks (17, 18). Thus, the automated MLT
 296 algorithm erroneously replaced the artefacts with bone HU values while the manual MLT
 297 correctly replaced the artefacts with metal HU values as shown in Figure (4). On the
 298 other hand, both MLT algorithms overestimated the RT hip where scatter and bright

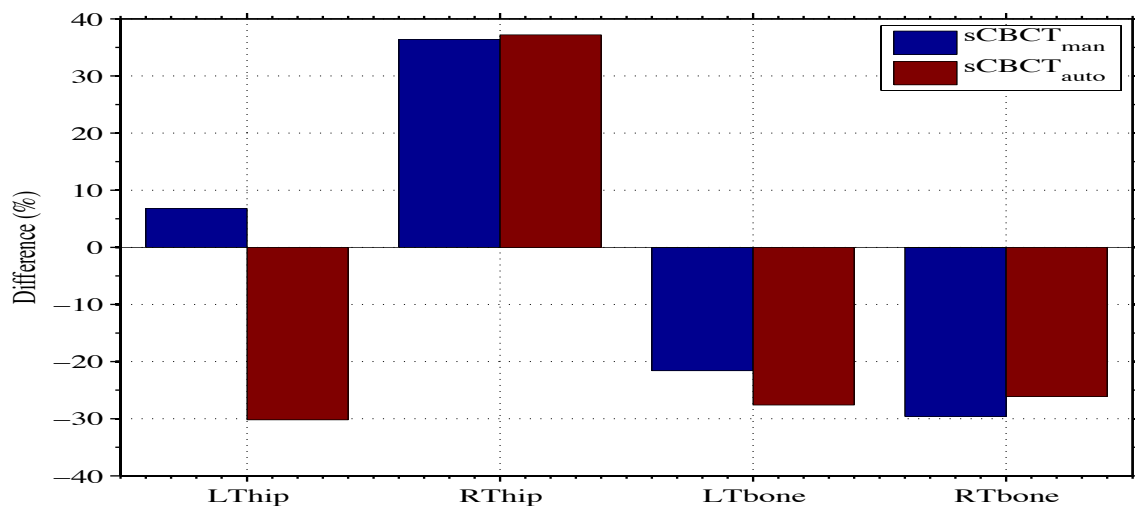


Figure 3: Right/Left hip and bone volume differences between pCT and $sCBCT_{man}/sCBCT_{auto}$.

299 streak artefacts were erroneously replaced with hip HU values, leading to a significant
300 reduction in the RT bone volume around that region. Another reason for the
301 underestimation of both bone volumes in both MLT algorithms might be due to the fact
302 that streak artefacts in pCT increased the number of high HU values and were not
303 corrected (only for dose calculation), where in sCBCT, both MLT algorithms attempted
304 to correct for this.

305

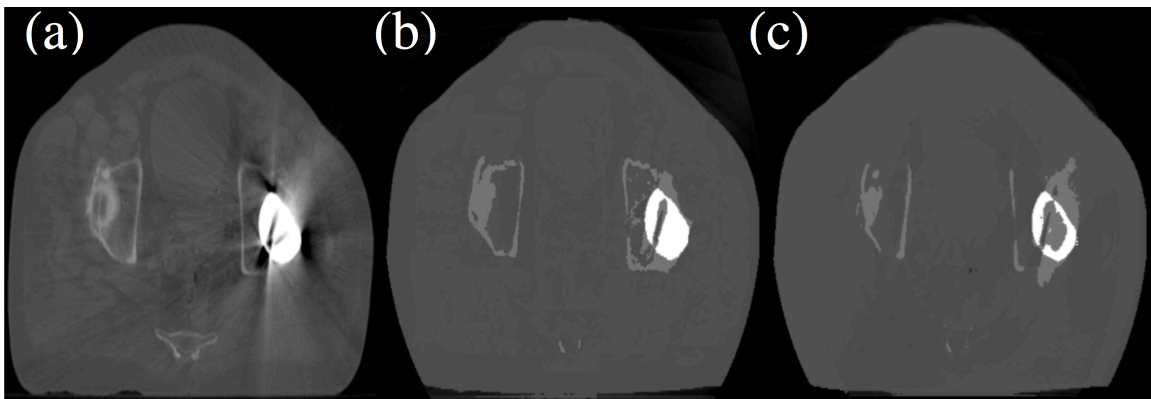


Figure 4: A slice of the pCT (a) and the resultant images after segmentation CBCT using the manual MLT (sCBCT_{man}) and the automated MLT (sCBCT_{auto}) (b and c respectively), showing the HU value difference in the left hip prosthesis.

306 Figure 5 shows the DVH of a prostate IMRT plan with a prescription dose of 70 Gy in
307 35 fractions. It shows the dose of the pCT, sCBCT_{man} and sCBCT_{auto} plans to the PTV,
308 rectum and bladder using the CC algorithm. Both sCBCT_{man} and sCBCT_{auto} plans
309 showed almost the same difference from the pCT plan, except for the PTV where
310 sCBCT_{man} showed better agreement, the difference in D_{max} between the pCT and
311 sCBCT_{man} plans was -0.56%, and sCBCT_{auto} was -1.4%. Compared with the pCT plan,
312 the sCBCT_{man} plan underestimated D_{mean} and D_{min} by -1% and -0.3%, respectively,
313 while the sCBCT_{auto} plan underestimated D_{mean} and D_{mean} by -1.6% and -1%,
314 respectively. The MC and PB algorithm showed similar results to CC algorithm (see

315 Table 1 in the Appendix 1). Compared with pCT plan, the bladder V65 was reduced by
 316 56% and 58% in sCBCT_{man} and sCBCT_{auto} plans, respectively, when using CC
 317 algorithm, showing better bladder sparing (Table 1). There was a tradeoff in the D95 of
 318 the PTV, which reduced by 9% and 14% in sCBCT_{man} and sCBCT_{auto} plans,
 319 respectively, when using the CC algorithm. Significant organ deformation was observed
 320 between the pCT and CBCT scans, especially in the bladder volume (>15% reduction).
 321 This deformation resulted in large differences in D_{mean} for the bladder in both sCBCT_{man}
 322 (-48.8%) and sCBCT_{auto} (-49.2%).

323 Previous studies used either deformable electron density or deformable image
 324 registration (DIR) to improve the dose calculation accuracy and to correct the uncertainty
 325 from organ de-formation (11, 14). For a standard prostate patient, the accuracy of dose
 326 calculation could be improved by 1-2% using these methods. Thor et al (2011) stated that
 327 the accuracy of DIR can be affected by bowel gas and artefacts from gold fiducial

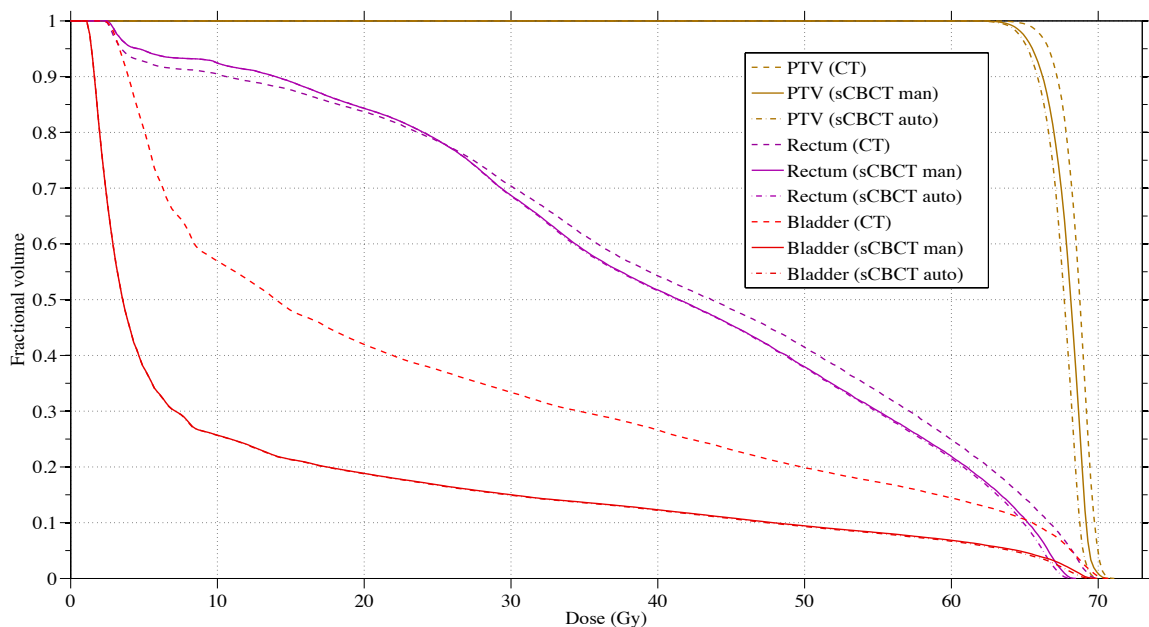


Figure 5: DVHs comparison pCT (-), sCBCT_{man} (-) and sCBCT_{auto} (-) IMRT plans for PTV, rectum and bladder using CC algorithm.

328 markers inside the prostate (23). Thus, in some cases, DIR would result in no
 329 improvement in the accuracy of the dose calculation (14). In this study, the image quality
 330 of both pCT and sCBCT images was affected by streak artefacts caused by the presence
 331 of the bilateral hip prostheses, thus the uncertainty associated with using DIR would be
 332 increased.

333 Table 1: PTV coverage for the pCT, sCBCT_{man} and sCBCT_{auto}. The dose to 95% of PTV
 334 volume and minimum dose and the percentage of rectal and bladder volumes receiving 65 Gy and
 335 70 Gy.

Scan		PTV		Rectum		Bladder	
		D95	Dmin	V65	V70	V65	V70
CT	PB	99.7	64.9	17.4	0.93	11.4	3.38
	CC	95.76	61.9	14.36	0	10.57	0.35
	MC	80.42	55.9	13.78	0	7	0
sCBCT _{man}	PB	94.51	62.5	12.83	0	5.13	0.52
	CC	86.99	61.7	10.74	0	4.6	0
	MC	80.13	55.9	10.36	0	4.2	0
sCBCT _{auto}	PB	92.99	62.1	12.25	0	4.96	0.3
	CC	82.1	61.3	9.66	0	4.39	0
	MC	75.65	53.5	9.26	0	4.01	0

336
 337 Dunlop et al (2015) eliminated the need for, and uncertainties associated with, DIR by
 338 acquiring pCT on the same day as the CBCT, to be used as the ground truth for dose
 339 calculation (9). Thus additional doses could be delivered to the patients.

340 Figure 6(a) shows the CI values of the pCT, sCBCT_{man} and sCBCT_{auto} plans using PB,
 341 CC and MC algorithms. In general, the differences in the CI values between pCT and
 342 sCBCT_{man} were smaller than those between pCT and sCBCT_{auto} using all algorithms.
 343 The difference of the CI values between pCT and sCBCT_{man} were -26.7 %, -42.8% and -

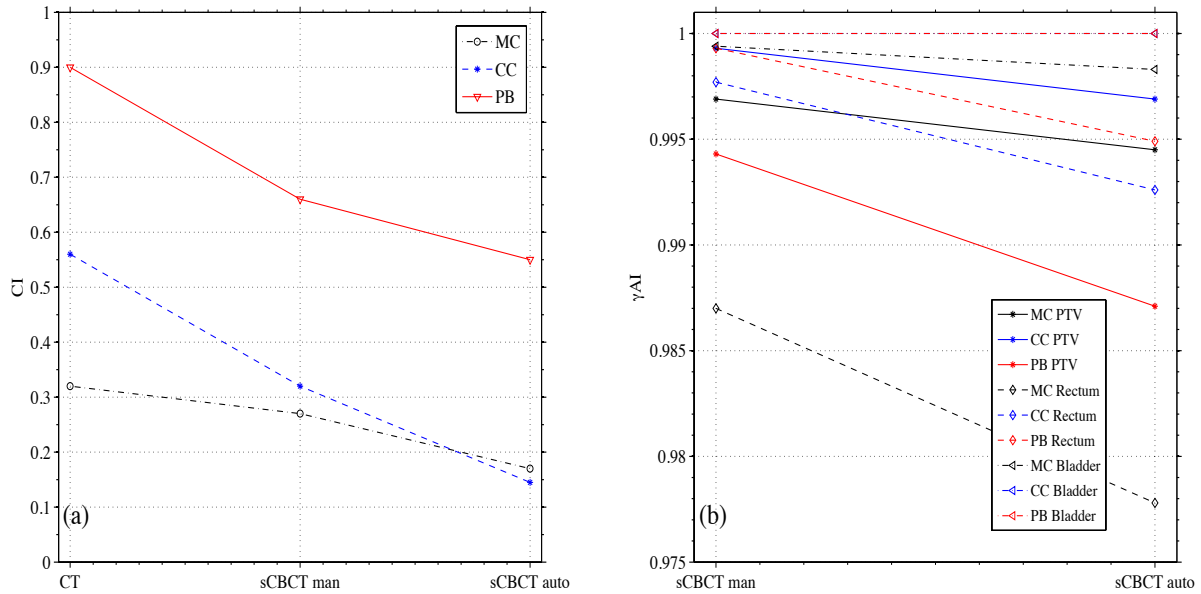


Figure 6: (a) Conformity index (CI) comparison between pCT, sCBCTman and sCBCTauto plans using PB, CC and MC algorithms. (b) Summary of the γ index with fixed DTA = 3 mm and DD = 3% for the calculation points falling inside the PTV, rectum and bladder, showing the fraction of points resulting with $\gamma < 1$.

344 15.6% when using PB, CC and MC algorithms, respectively. On the other hand, the
 345 difference of the CI values between pCT and sCBCT_{auto} were -38.9%, -74.1% and -
 346 46.9% when using PB, CC and MC algorithms, respectively. However, according to the
 347 RTOG guidelines, the CI values between 0.9 and 1 indicate that the target volume is not
 348 adequately covered by the prescribed isodose with a minor violation, whereas CI values
 349 of less than 0.9 the treatment plan are rated major violations but may nevertheless be
 350 considered to be acceptable (24).

351 Figure 6(b) shows the γ agreement index (γ AI) for the calculation points falling inside
 352 the PTV, rectum and bladder for the pCT, sCBCT_{man} and sCBCT_{auto} plans, showing the
 353 fraction of points resulting in $\gamma < 1$. For the bladder region, all the calculation points
 354 passed the gamma test when using the PB and CC algorithm, while using the MC
 355 algorithm, 99.9% and 99.8% showed $\gamma < 1$ for sCBCT_{man} and sCBCT_{auto}, respectively.

356 The lowest number of points that passed was found in the rectum region when using MC
 357 algorithm, where 98.7% showed $\gamma < 1$ in sCBCT_{man} and 97.7% showed $\gamma < 1$ in
 358 sCBCT_{auto} plans, which is clinically acceptable. Son et al stated that γ value is considered
 359 acceptable when the passing rate is greater than 95% with 3 mm DTA and 3% DD
 360 criteria (25).

361 Table 2: Dose comparison between pCT, sCBCT_{man} and sCBCT_{auto} plans at the isocentre using
 362 PB, CC and MC algorithms.

Scan	sCBCT _{man}			sCBCT _{auto}		
	PB	CC	MC	PB	CC	MC
Dose difference (%)	-0.81	-0.46	-0.39	-1.44	-1.36	-1.39

363
 364 Table 2 shows the dose difference between pCT and sCBCT plans at the isocentre using
 365 all algorithms. In general, both sCBCT_{man} and sCBCT_{auto} plans showed differences of
 366 less than -2% compared with the pCT plan using all algorithms, which are both
 367 considered to be clinically acceptable. It can be seen that the difference between the
 368 sCBCT_{man} and sCBCT_{auto} is larger when using CC and MC algorithms than that when
 369 using the PB algorithm. This is due to the fact that the PB algorithm in OMP calculates
 370 dose to water while, the CC algorithm calculates dose to medium, as does the MC
 371 algorithm (26). Therefore, the PB algorithm would be less sensitive than CC and MC for
 372 calculating the dose using different scans. Thus MC and CC algorithms minimised
 373 uncertainty related to the dose calculation as well as identifying those introduced by
 374 different scans. However, for the MC calculation, the difference increased from -0.4% in
 375 the sCBCT_{man} plan to -1.4% in sCBCT_{auto} plan when compared with the pCT plan. On

376 the other hand, the operator time required for defining the threshold values for different
377 regions in sCBCT_{man} was 8 hours while in sCBCT_{auto}, the threshold values were defined
378 automatically and takes 20 min operator time. Some manual modification to ensure an
379 appropriate assignment of each material in sCBCT_{auto} scan was still needed to improve
380 the accuracy but it requires much less (approximately 95%) operator time compared with
381 sCBCT_{man} scan. Dividing CBCT images into five concentric rings was accurate enough
382 to correct the variation in the pixel value with position in the CBCT images. As a result,
383 the automated MLT algorithm reduced the operator time with an acceptable accuracy.
384 This time saved could turn this technique from a research-based to a clinical
385 implementation and makes it superior compared with the manual approach. Compared
386 with the proposed technique in this paper, acquiring a new pCT is more time consuming,
387 increase work load on physicists, physicians, and radiographers, which can take up to a
388 day in a busy radiotherapy department, and more importantly additional dose is delivered
389 to the patient.

390 **4 Conclusion**

391 The segmentation of CBCT images using methods in this study can be used for dose
392 calculation. For a prostate patient with bilateral hip prostheses, the MLT algorithms
393 achieved a sufficient dose calculation accuracy that is clinically acceptable. The
394 automated MLT algorithm reduced the operator time associated with the MLT algorithm,
395 making it possible to implement the technique into clinic. Thus this method would be
396 feasible for ART, as an alternative to obtaining a new planning CT and re-outlining the
397 structures. This method can be applicable for dose calculation on MR images and could

398 be of interest to MR-based ART.

399

400

401

402

403

404

405

406

407

408

409

410

411

412

413

414 **Reference**

- 415 1. Langen KM, Jones DTL. Organ motion and its management. *International Journal*
416 *of Radiation Oncology* Biology* Physics*. 2001;50(1):265-78
- 417 2. Ciernik IF, Baumert BG, Egli P, Glanzmann C, Ltolf UM. On-line correction of
418 beam portals in the treatment of prostate cancer using an endorectal balloon
419 device. *Radiotherapy and oncology*. 2002;65(1):39-45.
- 420 3. Jaffray DA, Siewerdsen JH, Wong JW, Martinez AA. Flat-panel cone-beam
421 computed to- mography for image-guided radiation therapy. *International Journal*
422 *of Radiation Oncology* Biology* Physics*. 2002;53(5):1337-49.
- 423 4. Srinivasan K, Mohammadi M, Shepherd J. Cone beam computed tomography for
424 adaptive radiotherapy treatment planning. *Journal of Medical and Biological*
425 *Engineering*. 2014;34(4):377- 85.
- 426 5. Stock M, Pasler M, Birkfellner W, Homolka P, Poetter R, Georg D. Image quality
427 and stability of image-guided radiotherapy (IGRT) devices: A comparative study.
428 *Radiotherapy and Oncology*. 2009;93(1):1-7.
- 429 6. Fotina I, Hopfgartner J, Stock M, Steininger T, Ltgendorf-Caucig C, Georg D.
430 Feasibility of CBCT-based dose calculation: comparative analysis of HU
431 adjustment techniques. *Radiotherapy and Oncology*. 2012;104(2):249-56.
- 432 7. Richter A, Hu Q, Steglich D, Baier K, Wilbert J, Guckenberger M, et al.
433 Investigation of the usability of conebeam CT data sets for dose calculation.
434 *Radiat Oncol*. 2008;3(1):42.
- 435 8. Poludniowski GG, Evans PM, Webb S. Cone beam computed tomography
436 number errors and consequences for radiotherapy planning: an investigation of

- 437 correction methods. *International Journal of Radiation Oncology* Biology**
438 *Physics*. 2012;84(1):e109-e14.
- 439 9. Dunlop A, McQuaid D, Nill S, Murray J, Poludniowski G, Hansen VN, et al.
440 Comparison of CT number calibration techniques for CBCT-based dose
441 calculation. *Strahlentherapie und Onkologie*. 2015;191(12):970-8.
- 442 10. van Zijtveld M, Dirkx M, Heijmen B. Correction of conebeam CT values using a
443 planning CT for derivation of the dose of the day. *Radiotherapy and Oncology*.
444 2007;85(2):195-200.
- 445 11. Yang Y, Schreibmann E, Li T, Wang C, Xing L. Evaluation of on-board kV cone
446 beam CT (CBCT)-based dose calculation. *Physics in medicine and biology*.
447 2007;52(3):685-705.
- 448 12. Boggula R, Wertz H, Lorenz F, Madyan YA, Boda-Heggemann J, Schneider F, et
449 al. A proposed strategy to implement CBCT images for replanning and dose
450 calculations. *International Journal of Radiation Oncology* Biology* Physics*.
451 2007;69(3):S655-S6.
- 452 13. Boggula R, Lorenz F, Abo-Madyan Y, Lohr F, Wolff D, Boda-Heggemann J, et
453 al. A new strategy for online adaptive prostate radiotherapy based on cone-beam
454 CT. *Zeitschrift für Medizinische Physik*. 2009;19(4):264-76.
- 455 14. Onozato Y, Kadoya N, Fujita Y, Arai K, Dobashi S, Takeda K, et al. Evaluation
456 of OnBoard kV Cone Beam Computed Tomography-Based Dose Calculation
457 With Deformable Image Registration Using Hounsfield Unit Modifications.
458 *International Journal of Radiation Oncology* Biology* Physics*. 2014;89(2):416-
459 23.

- 460 15. Almatani T, Hugtenburg R, Lewis R, Barley S, Edwards M. Simplified material
461 assignment for cone beam computed tomography-based dose calculations of
462 prostate radiotherapy with hip prostheses. *Journal of Radiotherapy in Practice*.
463 2016;15(2):170-180.
- 464 16. Pineda AR, Siewerdsen JH, Tward DJ, editors. Analysis of image noise in 3D
465 cone-beam CT: Spatial and Fourier domain approaches under conditions of
466 varying stationarity. *Proc.SPIE* 2008; 6913: 69131Q-69131Q-10.
- 467 17. Shaw CC. *Cone beam computed tomography*: Taylor & Francis; 2014.
- 468 18. Bourland JD. *Image-guided Radiation Therapy*: Crc Press; 2012.
- 469 19. Kawrakow I, Rogers DWO. The EGSnrc code system. NRC Report PIRS-701,
470 NRC, Ottawa. 2000.
- 471 20. HPC Wales. Wales, UK. Available from: <http://www.hpcwales.co.uk/>.
472 [Accessed 08 December 15].
- 473 21. Deasy JO, Blanco AI, Clark VH. CERR: a computational environment for
474 radiotherapy research. *Medical physics*. 2003;30(5):979-85.
- 475 22. ICRU. International Commission on Radiation Units and Measurements.
476 Prescribing I. recording, and reporting photon-beam intensity-modulated
477 radiation therapy (IMRT). ICRU Report 83. *J icru*. 2010;10:1-106.
- 478 23. Thor M, Petersen JBB, Bentzen L, Hyer M, Muren LP. Deformable image
479 registration for contour propagation from CT to cone-beam CT scans in
480 radiotherapy of prostate cancer. *Acta Oncologica*. 2011;50(6):918-25.
- 481 24. Feuvret L, Nol G, Mazon J-J, Bey P. Conformity index: a review.

- 482 International Journal of Radiation Oncology* Biology* Physics.
483 2006;64(2):333-42.
- 484 25. Son J, Baek T, Lee B, Shin D, Park SY, Park J, et al. A comparison of the
485 quality assurance of four dosimetric tools for intensity modulated radiation
486 therapy. Radiology and oncology. 2015;49(3):307-13.
- 487 26. Knöös T, Wieslander E, Cozzi L, Brink C, Fogliata A, Albers D, et al.
488 Comparison of dose calculation algorithms for treatment planning in
489 external photon beam therapy for clinical situations. Physics in medicine
490 and biology. 2006;51(22):5785.

491

492

493

494

495

496

497

498

499

500

501

502

503 **List of Figures**

504 1. A slice of the pCT (a) and the original CBCT (b) and the resultant images after
505 segmentation CBCT using the manual MLT (sCBCT_{man}) and the automated
506 MLT(sCBCT_{auto}). 9

507 2. Comparison of the dose profile of pCT, sCBCT_{man} and sCBCT_{auto} plans at the
508 isocentre depth using MC algorithm. The second y axis represents the sCBCT_{man}
509 number, sCBCT_{auto} number and CT number. 12

510 3. Right/Left hip and bone volume differences between pCT and
511 sCBCT_{man}/sCBCT_{auto}. 13

512 4. A slice of the pCT (a) and the resultant images after segmentation CBCT using
513 the manual MLT (sCBCT_{man}) and the automated MLT (sCBCT_{auto}) (b and
514 c respectively), showing the HU value difference in the left hip prosthesis. 14

515 5. DVHs comparison pCT (-), sCBCT_{man} (-) and sCBCT_{auto} (-.) IMRT plans for
516 PTV, rectum and bladder using CC algorithm. 15

517 6. (a) Conformity index (CI) comparison between pCT, sCBCT_{man} and sCBCT_{auto}
518 plans using PB, CC and MC algorithm. (b) Summary of the γ index with fixed
519 DTA = 3 mm and DD = 3% for the calculation points falling inside the PTV,
520 rectum and bladder, showing the fraction of points resulting with $\gamma < 1$ 16

521 7. Dose comparison between pCT, sCBCT_{man} and sCBCT_{auto} plans at the isocentre
522 using PB, CC and MC algorithms. 17

523